THE JOURNAL OF BIOLOGICAL CHEMISTRY VOL. 290, NO. 8, pp. 4552–4559, February 20, 2015

Dimeric Quaternary Structure of Human Laforin*◆

Received for publication, November 25, 2014, and in revised form, December 17, 2014 Published, JBC Papers in Press, December 23, 2014, DOI 10.1074/jbc.M114.627406

Rajeshwer S. Sankhala[‡1], Adem C. Koksal[§1], Lan Ho[‡], Felix Nitschke[¶], Berge A. Minassian[¶‖], and Gino Cingolani[‡2]

From the [‡]Department of Biochemistry and Molecular Biology, Thomas Jefferson University, Philadelphia, Pennsylvania 19107, the [§]Department of Biological Chemistry and Molecular Pharmacology, Harvard Medical School, Boston, Massachusetts 02115, the [¶]Program in Genetics and Genome Biology, The Hospital for Sick Children, Toronto, Ontario M5G 1X8, Canada, and the [‖]Institute of Medical Sciences, Department of Pediatrics, University of Toronto, Ontario M5S 1A8, Canada

Background: Laforin is an essential glycogen phosphatase often mutated in Lafora disease.
Results: Human laforin adopts a dimeric quaternary structure.
Conclusion: Dimerization generates a unique active site crevice essential to recognize and dephosphorylate glycogen.
Significance: We derived a complete structural model of human laforin using hybrid structural methods.

The phosphatase laforin removes phosphate groups from glycogen during biosynthetic activity. Loss-of-function mutations in the gene encoding laforin is the predominant cause of Lafora disease, a fatal form of progressive myoclonic epilepsy. Here, we used hybrid structural methods to determine the molecular architecture of human laforin. We found that laforin adopts a dimeric quaternary structure, topologically similar to the prototypical dual specificity phosphatase VH1. The interface between the laforin carbohydrate-binding module and the dual specificity phosphatase domain generates an intimate substrate-binding crevice that allows for recognition and dephosphorylation of phosphomonoesters of glucose. We identify novel molecular determinants in the laforin active site that help decipher the mechanism of glucan phosphatase activity.

LD[3] is a fatal neurodegenerative disorder characterized by the intracellular accumulation of water-insoluble polyglucosan aggregates, known as Lafora bodies (1). These aggregates contain an aberrant form of glycogen that has reduced branching and is hyper-phosphorylated (2). Lafora bodies accumulate in the cytoplasm of several human tissues such as liver, skeletal muscle, heart, and brain (3), but although they are tolerated in most cells types, they cause progressive neuronal death. LD is caused by loss-of-function mutations in two genes, *EPM2A* (4, 5), which encodes the phosphatase laforin, and *EPM2B* (6), which encodes the E3 ubiquitin ligase malin (7). Over 60 known mutations in the laforin gene have been associated with LD (8). Similarly, mice lacking the laforin (9) or malin (10) gene form Lafora bodies and develop epilepsy.

The origin of glycogen phosphorylation in humans is unknown. Although plants possess several known starch kinases (11), a dedicated glycogen "kinase" has not been identified in metazoans. It was suggested (12) that glycogen accumulates phosphate at positions C2 and C3 of glucose as a result of the normal biosynthetic activity of glycogen synthase, which erroneously incorporates one phosphate moiety every ~10,000 glucose units. This finding was challenged by a recent report (2) that identified C6 as another major phosphorylation site in human glycogen. Because the mechanism proposed for glycogen phosphorylation by glycogen synthase cannot explain phospho-esterification at position C6 (12), alternative sources of glycogen phosphorylation are likely to exist. Laforin is the only glycogen phosphatase encoded in the human genome (13), and it is conserved in all vertebrates but absent in most invertebrate organisms, including model organisms such as yeast, flies, and worms (14). In this study, we used hybrid structural methods to characterize the three-dimensional organization of human laforin and to shed light on the mechanisms and regulation of glucan phosphatase activity.

EXPERIMENTAL PROCEDURES

Biochemical Techniques—Human laforin was cloned in vector pQE-80L lacking the N-terminal His tag. Laf-DSP (residues 150–331) and a synthetic gene encoding Laf-CBM (residues 1–137) (GenScript) were cloned in an engineered pET-28a vector containing an N-terminal maltose-binding protein gene. Point mutants C266S, C329S, C169S, R272A, R171A, D235A, and D197A were generated by site-directed mutagenesis. All proteins were expressed in *Escherichia coli* strain BL21 (DE3) RIL or Express I^q (New England Biolabs) cells by inducing at 20 °C for 12–16 h with 0.25 mM isopropyl 1-thio-β-D-galactopyranoside. Cell pellets were dissolved in Lysis buffer containing 50 mM HEPES, pH 7.5, 500 mM NaCl, 1 mM tris(2-carboxyethyl)phosphine (TCEP), 10% glycerol, 0.4% *n*-dodecyl β-D-maltoside, 1 mg ml^{-1} lysozyme, 80 μg ml^{-1} DNase, 1.0 mM phenylmethylsulfonyl fluoride and were disrupted by sonication. Recombinant proteins were purified on amylose beads (New England Biolabs), eluted from beads with 90 mM α-cD, and further purified on a Superose 12 gel filtration column (GE Healthcare) in GF1-buffer (25 mM HEPES, pH 7.5, 150 mM NaCl, 1 mM TCEP, 2% glycerol), as described previously (15).

* This work was supported by a Weizmann-Thomas Jefferson University Collaborative Pilot Program.
◆ This article was selected as a Paper of the Week.
The atomic coordinates and structure factors (code 4R30) have been deposited in the Protein Data Bank (http://wwpdb.org/).
[1] Both authors contributed equally to this work.
[2] To whom correspondence should be addressed: Dept. of Biochemistry and Molecular Biology, Thomas Jefferson University, 233 S. 10th St., Philadelphia, PA 19107. Tel.: 215-503-4573; E-mail: gino.cingolani@jefferson.edu.
[3] The abbreviations used are: LD, Lafora disease; DSP, dual specificity phosphatase; CBM, carbohydrate-binding module; TCEP, tris(2-carboxyethyl)-phosphine; α-cD, α-cyclodextrin; OMFP, 3-*O*-methylfluorescein phosphate; AUC, analytical ultracentrifugation; SV, sedimentation velocity; SAXS, small angle x-ray scattering.

Laf-DSP and laf-CBM were purified on amylose beads (New England Biolabs); maltose-binding protein was cleaved off with PreScission protease, and laforin domains were further purified by gel filtration on a Superdex 75 column (GE Healthcare) equilibrated in GF2-buffer (25 mM HEPES, pH 7.5, 100 mM NaCl, 3 mM β-mercaptoethanol). *In vitro* glucan phosphatase assay was carried out using 100 μg of amylopectin (Sigma) and 0.032 mg ml^{-1} laforin, as described (13, 16). Phosphate released upon hydrolysis was measured at 620 nm using the Malachite green reagent and quantified using a phosphate standard curve (17). Phosphatase kinetics with 3-*O*-methylfluorescein phosphate (OMFP) was measured using laforin at 0.0084 mg ml^{-1} as described (17, 18).

In Solution Biophysical Methods—Thermal stability assays were recorded using a Jasco J-810 spectropolarimeter equipped with a Neslab RTE7 refrigerated recirculator. Denaturing curves were measured by monitoring variations in ellipticity at 219 nm as a function of temperature, as described (19, 20). Laforin used in the assay was dissolved at 0.3 mg ml^{-1} in 20 mM sodium phosphate, pH 7.4, and 50 mM NaCl, 5 mM TCEP. Analytical ultracentrifugation (AUC) analysis was carried out in a Beckman XL-A analytical ultracentrifuge operating under velocity sedimentation (SV) mode as described (21, 22). Laforin samples were dissolved at 0.25–0.7 mg ml^{-1} in 25 mM HEPES, pH 7.5, 150 mM NaCl, 2% glycerol, 2 mM TCEP and were spun at 35,000 rpm at 20 °C. Absorbance values at 280 nm were fit to a continuous sedimentation coefficient ($c(s)$) distribution model in SEDFIT (23). Small angle x-ray scattering (SAXS) data were measured at the National Synchrotron Light Source beamline X9A by flowing protein samples through a capillary at a rate of 10 μl min^{-1}. Samples were dissolved in the GF1-buffer at concentrations ranging from 0.7 to 5.0 mg ml^{-1} for laforin and 2.25 to 3.75 mg ml^{-1} for laf-CBM; 20-s exposures were taken in triplicate. Data reduction was done by circular averaging of the images and scaling to obtain the scattering curve "scattering intensity (I)" as a function of the "momentum transfer vector q ($q = 4\pi(\sin\theta)/\lambda$)." GNOM (24) was used to calculate $P(r)$ plots from the scattering data. *Ab initio* model calculations to generate a scattering envelope were done using DAMMIN (25), and final solution models were converted to a surface map using SITUS (26). Docking of Protein Data Bank models inside the SAXS envelope was done manually and improved using SITUS (26), Sculptor (27), Chimera (28), and phenix.real_space_refine (29). Theoretical solution scattering curves were calculated using CRYSOL (30). The χ^2 for dimeric laforin ($\chi^2 = 3.02$) is acceptable but larger than that of laf-CBM ($\chi^2 = 0.83$). This is likely due to the intrinsic flexibility of the full-length protein, which cannot be perfectly represented by a single model. The correlation coefficient between the SAXS envelope and atomic model is 0.845 for laf-CBM and 0.806 for dimeric laforin.

Crystallographic Methods—Laf-DSP was crystallized using 0.10 M lithium sulfate, 0.05 M sodium cacodylate, pH 6.5, 0.1 M NaCl, 10 mM TCEP, at 18 °C. Crystals were cryo-protected with 30% ethylene glycol, flash-frozen in liquid nitrogen, and diffracted at beamlines X6A and X29 at the National Synchrotron Light Source. Data reduction was done with the HKL2000 (Table 1) (31), and the structure was solved by molecular replacement and structure modeling in Rosetta using PTPMP1 (Protein Data Bank 3RGO) as the initial search model, as implemented in phenix.mr_rosetta (32). This solution was subjected to autobuilding and refinement in Phenix (33) and COOT (34). The final model has an R_{work}/R_{free} of 18.8/21.9% (using all data between 15 and 2.30 Å resolution) and excellent geometry (Table 1). The sulfhydryl groups of Cys-250, Cys-278, and Cys-329 are covalently bound β-mercaptoethanol (data not shown).

RESULTS

"Divide and Conquer" Approach to Study Laforin Structure—Laforin has a bipartite organization that consists of an N-terminal CBM spanning residues 1–130 and a C-terminal DSP domain (residues 150–331) (Fig. 1*A*). Although laforin is partially membrane-bound *in vivo* (35), the protein can be extracted from lipids using nonionic detergents and solubilized with carbohydrates. *In vitro*, purified laforin is stabilized upon binding to carbohydrates that enhance its solubility by burying hydrophobic residues in the CBM (36). We measured an apparent melting temperature ($T_{m,\,app}$) of 62 °C for purified laforin bound to α-cD and 68 °C in the presence of maltose; on the contrary, removing carbohydrates by prolonged dialysis reduced laforin stability and made the protein aggregation-prone (Fig. 1*B*). Because laforin failed to crystallize as a full-length protein, we expressed and purified individual DSP and CBM domains in large quantity for crystallization and studied the full-length laforin in solution using SAXS, AUC-SV, and phosphatase assay.

Crystal Structure of Laforin DSP Domain—We crystallized an inactive mutant (C266S) of laforin DSP (laf-DSP) spanning residues 150–331, and we determined its structure to an R_{work}/R_{free} of 18.8/21.9%, at 2.3 Å resolution (Table 1). Laf-DSP consists of a central five-stranded β-sheet (β1 to β5) sandwiched between two clusters of seven α-helices (α1 to α3 and α4 to α7), similar to the prototypical DSP VH1 (Fig. 1*C*) (21). The laforin catalytic triad consists of Cys-266 (the catalytic residue), Arg-272 (the general base), and Asp-235 (the general acid); the first two residues are part of a phosphate-binding loop, or "P-loop" (residues 265–272), whereas Asp-235 is located in a separate loop, the "general acid" loop (residues 230–238). Secondary structure alignment of laf-DSP with the starch phosphatase Sex4 (37) (root mean square deviation of 2.4 Å) and the phosphoinositide phosphatase PTEN (38) (root mean square deviation of 2.6 Å) reveals a superimposable position of the catalytic cysteine and general base, whereas the laforin general acid Asp-235 is shifted away from the active site (7.9 Å *versus* ~3.5 Å) (Fig. 1*C*). The open conformation of the laforin general acid loop is stabilized by the bulky side chain of Tyr-304 that projects from the surface of the "TI-loop" (residues 296–307) (Fig. 1*D*). The laforin "E-loop" is also significantly longer than in the other two phosphatases and contains an inserted helix, α2 (Fig. 1*D*). Overall, the laforin active site crevice is wide and shallow (~6 Å), with a calculated solvent-excluded surface for Cys-266 of only 7.1 Å^2, lower than Cys-152 in Sex4 (110.5 Å^2) and Cys-110 in PTEN (65.0 Å^2). Laf-DSP also contains a second surface-exposed pocket, ~6 Å in depth, adjacent to the active site (Fig. 1*E*). Three residues lining this pocket, Cys-169, Arg-171, and Asp-197, form a "second" triad,

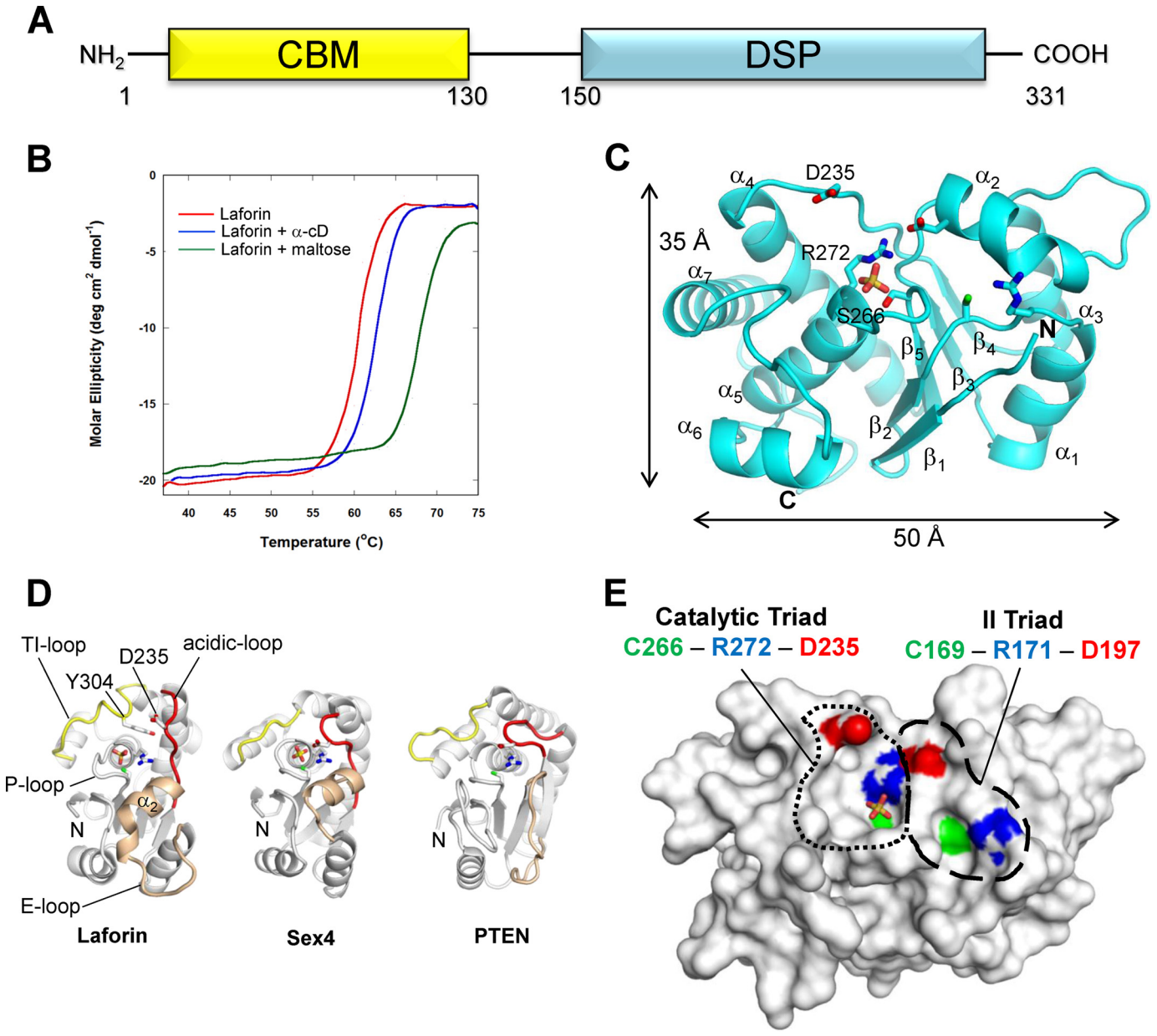

FIGURE 1. **Crystal structure of laforin DSP.** *A*, schematic diagram of laforin domain organization. *B*, thermal stability of apo-laforin (*red line*) and in the presence of α-cD (*blue line*) or maltose (*green line*). The $T_{m,\,app}$ is 60 °C for apo-laforin, 62 °C in the presence of 5 mM α-cD, and 68 °C in the presence of 10 mM maltose. *C*, ribbon representation of laf-DSP with catalytic triad, second triad, and active site sulfate ion shown as *sticks*. *D*, top views of the laf-DSP (residues 150–331), plant Sex4-DSP (residues 96–249) (37), and human PTEN-DSP (residues 23–185) (38) highlighting critical loops surrounding the active site. *E*, surface representation of laf-DSP is as follows: catalytic and second triads are *circled* with *dashed lines*. Cys-266/Cys-169, Arg-272/Arg-171, and Asp-235/Asp-197 are colored in *green, blue,* and *red*, respectively.

similar in topology to the catalytic triad. The two triads appear to cross-talk structurally in two respects. First, Cys-169 and the catalytic Cys-266 are equidistant (~3 Å) from a histidine (His-265), which in classical phosphotyrosine phosphatases is known to decrease the active site cysteine pK_a, promoting formation of a thiolate intermediate at physiological pH (39). Second, Asp-197 makes a bidentate salt bridge with the guanidinium group of the general base Arg-272. Thus, the crystallographic structure of laf-DSP reveals a classical phosphotyrosine phosphatase-fold characterized by an unusually broad and shallow active site crevice and an open conformation of the general acid loop.

SAXS-restrained Model of Laforin CBM Bound to α-cD—Unlike the phosphatase domain, we were not able to crystallize laf-CBM. We then generated a homology model of this conserved domain (Fig. 2*A*) using the prediction server I-TASSER (40), which uses multiple-threading alignments and iterative template fragment assembly simulations. We also measured the SAXS profile of human laf-CBM in the presence of 10 mM α-cD and calculated an *ab initio* SAXS envelope using scattering data at 3.2 mg ml^{-1} concentration. Laf-CBM SAXS envelope is shaped like a "pear," with a tapered and a bulgy end, and it is slightly curved when rotated by 90° (Fig. 2*A*). Laf-CBM homology model was docked inside the SAXS density, and the

position of α-cD was determined by superimposing laf-CBM to the structure of the *Aspergillus niger* CBM20 bound to β-cD (Protein Data Bank code 1ACZ) (41). The composite laf-CBM model bound to α-cD was then refined against the SAXS envelope using low resolution real space refinement. The excellent agreement of distance distribution functions ($P(r)$) calculated from experimental SAXS data and laf-CBM·α-cD complex (Fig. 2*B*) suggest our model of laf-CBM is reasonably accurate.

Solution Structure of Human Laforin—To investigate the oligomeric state of human laforin, we subjected purified laforin to AUC-SV analysis in a range of concentrations (0.25–0.7 mg ml^{-1}). At physiological salt and in the presence of reducing agents, laforin migrated as a homogeneous species with apparent sedimentation coefficient (s*) of 3.85 S, corresponding to a dimer of ~71.1 kDa (expected mass of 74.2 kDa) (Fig. 3*A* and Table 2). A C329S mutant of laforin had nearly identical s* (Table 2), ruling out the involvement of Cys-329 in dimerization (42). Likewise, SAXS spectra measured at a concentration of laforin between 0.7 and 5.0 mg ml^{-1} gave a gyration radius and maximum diameter of 33.4 and 115.0 Å, respectively, remarkably close to the Stokes radius calculated from SV analysis and fully consistent with a dimeric quaternary structure (Table 2).

To visualize the structural organization of dimeric laforin, we generated an *ab initio* shape reconstruction from scattering data at 2.0 mg ml^{-1}. Laforin's SAXS envelope revealed an ellipsoidal shape characterized by three lobes of density (Fig. 3*B*), which we interpreted using the structures of laf-DSP and laf-CBM described above. The external lobes in the SAXS envelope are rotated by 75° with respect to each other and each fit one DSP domain; the central lobe instead is too large for one DSP but accommodates a dimer of laf-CBMs arranged in a parallel fashion (Fig. 3*B*). This quaternary structure yields excellent agreement of $P(r)$ functions calculated from experimental SAXS data and the proposed model (Fig. 3*C*). Some ambiguity remains in the way laf-DSPs connect to CBMs that could be swapped, like in VH1 (18, 21), or juxtaposed, although either topology generates an equivalent quaternary structure. Mapping sugar-binding residues in this model using the structure of Sex4 bound to maltoheptaose (37) as a template and knowledge of LD mutations that disrupt sugar binding (8) identified two contiguous clusters of amino acids, one in the CBM (Trp-32, Phe-84, Trp-85, Lys-87, Trp-99, and His-105) and the other in the DSP (Gln-200, Asn-201, Met-236, Arg-241, Lys-299, and Arg-300). The two clusters face each other in our model (Fig. 3*D*) generating a narrow pocket that sandwiches a bound glucan, presenting it to the phosphatase active site. This model also explains the high affinity of laforin for glucan chains and its preference for phosphoglucose over peptidic substrates.

Dimerization Triggers Laforin Catalytic Activity—To dissect the structural basis for glucan phosphatase activity, we mutated each of the residues in the laforin catalytic triad (Cys-266, Arg-272, and Asp-235) and second triad (Cys-169, Arg-171, and Asp-197) (Fig. 1*E*), and we measured the phosphatase activity of these mutants toward potato amylopectin and OMFP. Although laf-DSP was completely inactive, dimeric wild type (WT) laforin efficiently dephosphorylated amylopectin (Fig. 4*A*) and OMFP ($k_{cat}/K_m = 1.90 \times 10^8$ M^{-1} s^{-1} and $K_m = 520 \pm$

TABLE 1
Crystallographic data collection and refinement statistics
Values in parentheses are for highest resolution shell.

	Laforin DSP
Data collection	
Beamline	X29
Wavelength (Å)	1.07
Space group	$I\,4_1$
Cell dimensions	
a, *b*, *c* (Å)	123.9, 123.9, 160.7
α, β, γ (°)	90.0, 90.0, 90.0
Unique reflections	52,012
Completeness, %	97.1 (88.3)
Resolution (Å)	15.0-2.3 (2.4-2.3)
R_{sym}	9.6 (53.0)
Redundancy	2.9 (2.2)
I/σ_I	19.3 (1.9)
Wilson B factor	46.5
Refinement	
Resolution limits (Å)	15.0-2.3
No. of reflections	51,890
R_{work}/R_{free} [a]	18.8/21.9
No. of protein residues	716
No. of solvent molecules	243
No. of β-ETOH/ions	12/4
B-Factor	
Protein atoms	59.7
Sulfate ions	55.9
Waters	54.1
Ramachandran plot (%) core/allowed/generally allowed/disallowed	89.5/9.9/0.6/0.0
Root mean square deviations from ideal	
Bond lengths (Å)	0.008
Bond angles (°)	1.159

[a] The R_{free} value was calculated using 1,969 randomly selected reflections.

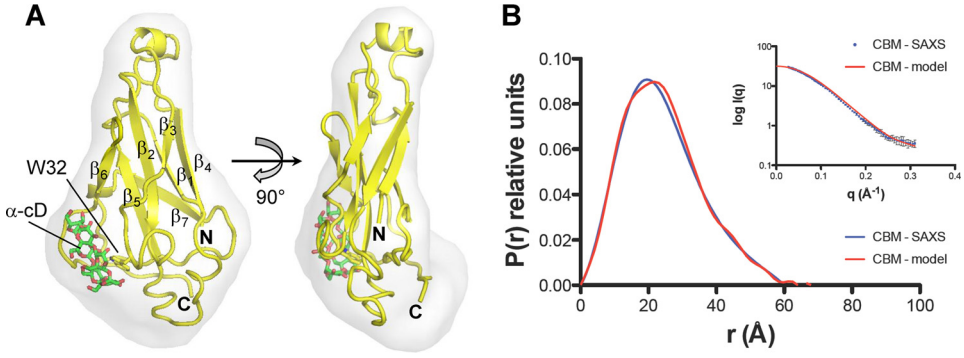

FIGURE 2. **SAXS-restrained model of laforin CBM bound to α-cD.** *A, ab initio* SAXS reconstructions of laf-CBM (in *gray*) calculated from experimental scattering values at 3.2 mg ml^{-1}. Overlaid to the SAXS envelope is a homology model of human laf-CBM. *B,* agreement of $P(r)$ functions calculated from experimental SAXS data (*blue*) and data calculated from the laf-CBM model (*red*). *Inset* shows experimental scattering data (*blue*) overlaid to the scattering curve calculated from the laf-CBM model (*red*).

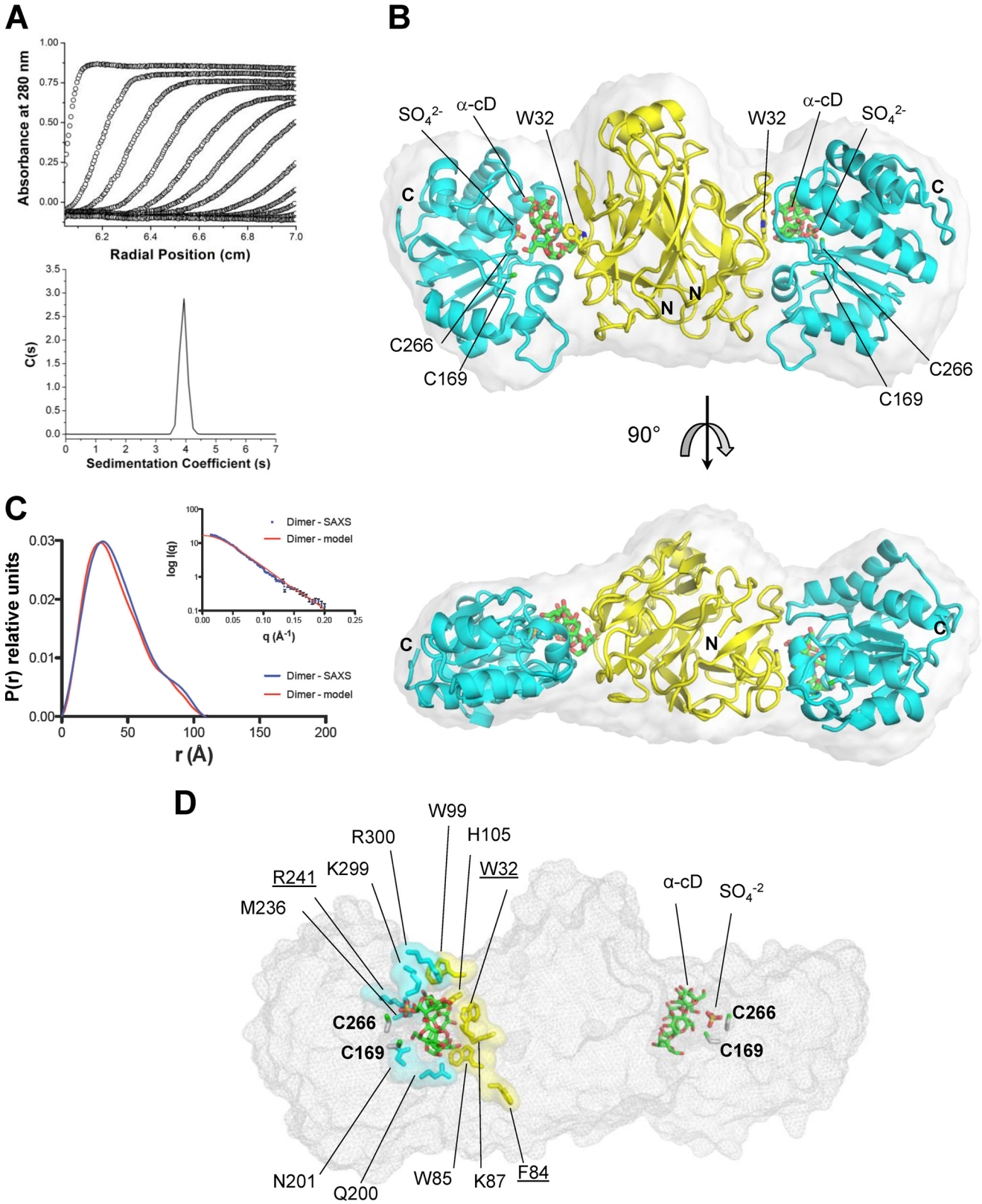

FIGURE 3. **Quaternary structure of human laforin.** *A,* sedimentation velocity profiles of human laforin at 20 °C. *Top panel,* raw absorbance at 280 nm plotted as a function of the radial position. Data at intervals of 60 min are shown as *open circles* for sedimentation at 35,000 rpm. *Bottom panel,* fitted distribution of s*. *B, ab initio* SAXS reconstruction of dimeric laforin (*light gray*) displayed in side and top views overlaid to a pseudo-atomic model of the enzyme obtained by docking ribbon models of laf-DSP and laf-CBM inside the SAXS envelope. *C,* agreement of *P*(*r*) functions calculated from experimental SAXS data (*blue*) and data calculated from the pseudo-model (*red*) of dimeric laforin. *Inset,* experimental scattering data (*blue*) overlaid to the scattering curve calculated from the laforin model (*red*). *D,* a model of dimeric laforin (*gray mesh*) bound to α-cD (*green*): carbohydrate-binding residues projecting from laf-CBM (in *yellow*) and laf-DSP (*cyan*) (shown only for one active site), as well as Cys-266/Cys-169, and sulfate ions are shown as *thick sticks*. *Underlined* are residues mutated in LD (8).

35 μM) (Fig. 4*B*), with 2 orders of magnitude higher catalytic efficiency than the prototypical DSP VH1 (18, 21). Substitutions at Cys-266 and Arg-272 completely disrupted phosphatase activity (Fig. 4, *A* and *B*) consistent with the essential role played by these two residues. Unlike Cys-266 and Arg-272, laforin general acid Asp-235 had not been validated in a phosphatase assay. Given the open conformation of the laforin acidic loop (Fig. 1*C*), we reasoned this loop may either close upon binding to a phospho-substrate to bring Asp-235 closer to the active site or laforin phosphatase activity could be independent of a general acid, as reported for PIR1 (17) and PTEN (38). To test this hypothesis, we mutated Asp-235 to alanine and found that laforin-D235A was inactive as glucan phosphatase (Fig. 4*A*) and had ~9.0-fold reduced turnover number for OMFP compared with WT-laforin (k_{cat} = 11,144 s^{-1} *versus* 99,830 s^{-1}, Fig. 4*B*) consistent with a slower enzyme. The affinity of D235A for OMFP was apparently increased by the alanine mutation (K_m = 60 ± 2 μM). This is possibly explained by a decreased dissociation constant between enzyme and substrate (k_{-1}) due to the inability of this mutant to release the covalent phosphoenzyme intermediate, which decreases the Michaelis-Menten constant (defined as $K_m = (k_{-1} + k_2)/k_1$).

Next, we examined the effect of mutations in the second triad. Mutation of Cys-169 and Arg-171 reproducibly reduced glucan phosphatase activity by 6 and 12%, respectively (Fig. 4*A*), without decreasing laforin specificity (K_m = 580 ± 10 μM and K_m = 400 ± 20 μM) and catalytic efficiency ($k_{cat}/K_m = 1.53 \times 10^8$ M^{-1} s^{-1} and $k_{cat}/K_m = 2.70 \times 10^8$ M^{-1} s^{-1}) toward OMFP (Fig. 4*B*). In contrast, D197A completely disrupted laforin activity (Fig. 4, *A* and *B*) possibly because mutations of acidic residues stabilizing the general base severely affect catalytic activity (43). Importantly, none of these mutations reduced laforin structural stability, as assessed from their heat-induced denaturation curves (data not shown). Thus, mutations in the second triad also affect laforin phosphatase activity, suggesting an active involvement of these residues in glycogen dephosphorylation.

TABLE 2
Biophysical parameters measured using AUC and SAXS

AUC	Laforin		Laforin-C329S	
Apparent Sedimentation coefficient, s* (S)	3.85		3.90	
Absolute Sedimentation coefficient, $S_{20,w}$ (S)	4.49		4.55	
Estimated/Expected Molecular Weight, MW (kDa)	71.1/74.2		71.2/74.2	
Frictional Ratio, f/f_0	1.35		1.37	
Stokes Radius, R_H (Å)	36.90		37.60	
SAXS	**Observed**	**Model**		
Gyration Radius, (Å)	33.4	30.5		
Maximum Diameter, D_{max} (Å)	115.0	109.0		
Molecular Weight, MW (kDa)	69.2	74.2		

DISCUSSION

Over a century after the discovery of LD (1), and nearly 2 decades since the identification of the laforin gene (4), we have derived a complete structural model of human laforin using hybrid structural methods. This structure provides clues to understanding laforin glycogen phosphatase activity, important to decipher the molecular etiology of LD.

The oligomeric state of human laforin has been controversial with reports of laforin forming a monomer (44), a dimer (45, 46), and even a cross-linked dimer (42). Combining the power of AUC-SV with SAXS and folding studies, we found that laforin folds into a stable homodimer in a range of concentrations between 0.25 and 5.0 mg ml^{-1} (Fig. 3, *A* and *B*). This supports previous findings by Liu *et al.* (45) and contradicts a recent report that laforin is monomeric based solely on size exclusion chromatography (44). Our structural analysis reveals that the laforin quaternary structure is stabilized by dimerization of its N-terminal CBM (Fig. 3*B*). This is analogous to how VH1 assembles into a dimer by swapping an N-terminal helix (18, 21). As observed for VH1 (18, 21), and reported for laforin (45),

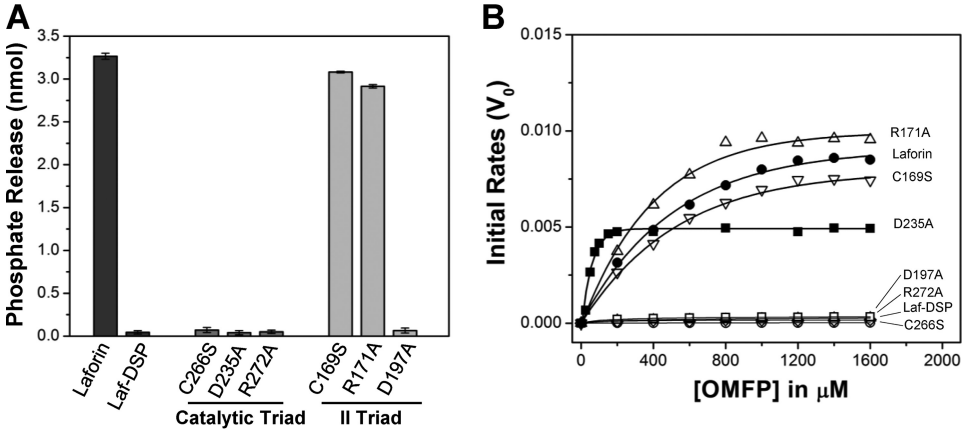

FIGURE 4. **Catalytic activity of dimeric laforin toward amylopectin and OMFP.** *A,* dephosphorylation of 100 μg of amylopectin by various point mutants of laforin and laf-DSP. *Error bars* are based on three independent repeats. *B,* Michaelis-Menten saturation kinetics of dimeric laforin for OMFP. Initial rates of OMFP hydrolysis by various laforin mutants are plotted against OMFP concentration, which ranges between 0 and 1600 μM. Kinetic parameters measured in this experiment are as follows: WT laforin (●): K_m = 520.0 ± 35.0 μM, V_{max} = 0.012, k_{cat} = 99,830 s^{-1}, $k_{cat}/K_m = 1.90 \times 10^8$ M^{-1} s^{-1}; C169S (▽): K_m = 580.0 ± 10.0 μM, V_{max} = 0.01, k_{cat} = 88,641 s^{-1}, $k_{cat}/K_m = 1.53 \times 10^8$ M^{-1} s^{-1}; R171A (△): K_m = 400.0 ± 20.0 μM, V_{max} = 0.013, k_{cat} = 109,425 s^{-1}, $k_{cat}/K_m = 2.70 \times 10^8$ M^{-1} s^{-1}; D235A (■): K_m = 60.0 ± 2.0 μM, V_{max} = 0.006, k_{cat} = 11,144 s^{-1}, $k_{cat}/K_m = 1.85 \times 10^8$ M^{-1} s^{-1}. Mutants D197A, R272A, C266S, and laf-DSP did not show detectable activity.

dimerization is essential for catalytic affinity. Whereas the isolated DSP domain of laforin is inactive *in vitro*, the dimeric full-length protein is highly active toward glucans and OMFP (Fig. 4, *A* and *B*). We propose that dimerization leads to laforin activation in two ways. First, it induces intramolecular contacts between DSP and CBM that force the acidic loop closer to the active site, in a conformation poised for acid-base catalysis. Second, it closes the sugar-binding pocket positioning a bound glucan between two clusters of carbohydrate-binding residues, thereby reducing the rate of substrate dissociation from the active site (Fig. 3*D*). However, swapping laf-DSP with VH1-related (VHR) results in a phosphatase inactive toward polyglucosan (47), suggesting that CBM-induced dimerization and activation of phosphatase activity are necessary but not sufficient to promote laforin glucan phosphatase activity, which depends on unique structural determinants in laf-DSP. In a quest for these determinants, we identified a second surface-exposed pocket next to the laforin active site lined by three residues strikingly similar to the catalytic triad (Fig. 1*E*). Our mutational analysis suggests the second triad is also important for laforin glucan phosphatase activity; disrupting either Cys-169 or Arg-171 results in a modest yet reproducible decrease in glucan phosphatase activity, although mutation of Asp-197 completely disrupts phosphatase activity (Fig. 4*A*). Although it may be argued that most point mutations of surface-exposed residues next to the active site destabilize substrate binding, mutations at Cys-169 and Arg-171 did not decrease laforin affinity for OMFP (Fig. 4*B*). We propose that laforin second triad functions in synergy with the catalytic triad possibly by dephosphorylating different phosphomonoesters of glucose. Unfortunately, the amylopectin phosphatase assay is poorly sensitive, and unlike glycogen, amylopectin lacks phosphate groups at position Cys-2 (2, 48), arguing that laforin-C266S, thus far thought to be a catalytically dead mutant, could indeed harbor residual activity. To corroborate the dichotomy between laforin activity toward amylopectin *in vitro* and glycogen phosphatase activity *in vivo*, a missense point mutation at position Arg-171 causes LD *in vivo* (8), whereas an alanine mutation at this position decreased amylopectin dephosphorylation only by 12% (Fig. 4*A*). Thus, even a modest deficiency in phosphatase activity *in vitro* may result in devastating changes in brain glycogen phosphorylation *in vivo*. Our structural finding of a second triad immediately next to the laforin active site may help resolve a major conundrum in the field raised by a recent well founded report that overexpression of laforin-C266S in laforin-deficient mice wholly rescues LD (49), suggesting that the phosphatase activity of laforin, its only known enzymatic activity, is irrelevant. We propose that laforin's second triad harbors residual catalytic activity, which sufficiently dephosphorylates glycogen when laforin-C266S is overexpressed (49). The absence of laforin-C266S *in vitro* phosphatase activity could imply that the second triad requires conditions that are only maintained *in vivo*, in nondividing cells like neurons.

In conclusion, the long-sought structure of human laforin presented in this study sheds light on the molecular basis for glycogen dephosphorylation and sets the ground for future investigations to validate a putative second phosphatase active site.

Acknowledgment—We are grateful to the staff at the National Synchrotron Light Source beamlines X6A, X29, and X9 for assistance in data collection. Research in this publication includes work carried out at the Sydney Kimmel Cancer Center X-ray Crystallography and Molecular Interaction Facility, which is supported in part by NCI Grant P30 CA56036.

REFERENCES

1. Lafora, G., and Glick, G. (1911) Beitrag zur histopathologie del myoklonischen epilepsie. *Z. Ges. Neurol. Psychiatr.* **6,** 1–14
2. Nitschke, F., Wang, P., Schmieder, P., Girard, J. M., Awrey, D. E., Wang, T., Israelian, J., Zhao, X., Turnbull, J., Heydenreich, M., Kleinpeter, E., Steup, M., and Minassian, B. A. (2013) Hyperphosphorylation of glucosyl C6 carbons and altered structure of glycogen in the neurodegenerative epilepsy Lafora disease. *Cell Metab.* **17,** 756–767
3. Minassian, B. A. (2002) Progressive myoclonus epilepsy with polyglucosan bodies: Lafora disease. *Adv. Neurol.* **89,** 199–210
4. Minassian, B. A., Lee, J. R., Herbrick, J. A., Huizenga, J., Soder, S., Mungall, A. J., Dunham, I., Gardner, R., Fong, C. Y., Carpenter, S., Jardim, L., Satishchandra, P., Andermann, E., Snead, O. C., 3rd, Lopes-Cendes, I., Tsui, L. C., Delgado-Escueta, A. V., Rouleau, G. A., and Scherer, S. W. (1998) Mutations in a gene encoding a novel protein tyrosine phosphatase cause progressive myoclonus epilepsy. *Nat. Genet.* **20,** 171–174
5. Serratosa, J. M., Gómez-Garre, P., Gallardo, M. E., Anta, B., de Bernabé, D. B., Lindhout, D., Augustijn, P. B., Tassinari, C. A., Malafosse, R. M., Topcu, M., Grid, D., Dravet, C., Berkovic, S. F., and de Córdoba, S. R. (1999) A novel protein tyrosine phosphatase gene is mutated in progressive myoclonus epilepsy of the Lafora type (EPM2). *Hum. Mol. Genet.* **8,** 345–352
6. Chan, E. M., Young, E. J., Ianzano, L., Munteanu, I., Zhao, X., Christopoulos, C. C., Avanzini, G., Elia, M., Ackerley, C. A., Jovic, N. J., Bohlega, S., Andermann, E., Rouleau, G. A., Delgado-Escueta, A. V., Minassian, B. A., and Scherer, S. W. (2003) Mutations in NHLRC1 cause progressive myoclonus epilepsy. *Nat. Genet.* **35,** 125–127
7. Gentry, M. S., Worby, C. A., and Dixon, J. E. (2005) Insights into Lafora disease: malin is an E3 ubiquitin ligase that ubiquitinates and promotes the degradation of laforin. *Proc. Natl. Acad. Sci. U.S.A.* **102,** 8501–8506
8. Singh, S., and Ganesh, S. (2009) Lafora progressive myoclonus epilepsy: a meta-analysis of reported mutations in the first decade following the discovery of the EPM2A and NHLRC1 genes. *Hum. Mutat.* **30,** 715–723
9. Ganesh, S., Delgado-Escueta, A. V., Sakamoto, T., Avila, M. R., Machado-Salas, J., Hoshii, Y., Akagi, T., Gomi, H., Suzuki, T., Amano, K., Agarwala, K. L., Hasegawa, Y., Bai, D. S., Ishihara, T., Hashikawa, T., Itohara, S., Cornford, E. M., Niki, H., and Yamakawa, K. (2002) Targeted disruption of the Epm2a gene causes formation of Lafora inclusion bodies, neurodegeneration, ataxia, myoclonus epilepsy and impaired behavioral response in mice. *Hum. Mol. Genet* **11,** 1251–1262
10. Turnbull, J., Wang, P., Girard, J. M., Ruggieri, A., Wang, T. J., Draginov, A. G., Kameka, A. P., Pencea, N., Zhao, X., Ackerley, C. A., and Minassian, B. A. (2010) Glycogen hyperphosphorylation underlies lafora body formation. *Ann. Neurol.* **68,** 925–933
11. Hejazi, M., Fettke, J., Kötting, O., Zeeman, S. C., and Steup, M. (2010) The laforin-like dual-specificity phosphatase SEX4 from *Arabidopsis thaliana* hydrolyses both C6- and C3-phosphate esters introduced by starch-related dikinases and thereby affects phase transition of α-glucans. *Plant Physiol.* **152,** 711–722
12. Tagliabracci, V. S., Heiss, C., Karthik, C., Contreras, C. J., Glushka, J., Ishihara, M., Azadi, P., Hurley, T. D., DePaoli-Roach, A. A., and Roach, P. J. (2011) Phosphate incorporation during glycogen synthesis and Lafora disease. *Cell Metab.* **13,** 274–282
13. Tagliabracci, V. S., Turnbull, J., Wang, W., Girard, J. M., Zhao, X., Skurat, A. V., Delgado-Escueta, A. V., Minassian, B. A., Depaoli-Roach, A. A., and Roach, P. J. (2007) Laforin is a glycogen phosphatase, deficiency of which

leads to elevated phosphorylation of glycogen *in vivo*. *Proc. Natl. Acad. Sci. U.S.A.* **104,** 19262–19266
14. Gentry, M. S., Dowen, R. H., 3rd, Worby, C. A., Mattoo, S., Ecker, J. R., and Dixon, J. E. (2007) The phosphatase laforin crosses evolutionary boundaries and links carbohydrate metabolism to neuronal disease. *J. Cell Biol.* **178,** 477–488
15. Lokareddy, R. K., Bhardwaj, A., and Cingolani, G. (2013) Atomic structure of dual-specificity phosphatase 26, a novel p53 phosphatase. *Biochemistry* **52,** 938–948
16. Worby, C. A., Gentry, M. S., and Dixon, J. E. (2006) Laforin, a dual specificity phosphatase that dephosphorylates complex carbohydrates. *J. Biol. Chem.* **281,** 30412–30418
17. Sankhala, R. S., Lokareddy, R. K., and Cingolani, G. (2014) Structure of human PIR1, an atypical dual-specificity phosphatase. *Biochemistry* **53,** 862–871
18. Koksal, A. C., and Cingolani, G. (2011) Dimerization of vaccinia virus VH1 is essential for dephosphorylation of STAT1 at tyrosine 701. *J. Biol. Chem.* **286,** 14373–14382
19. Olia, A. S., Bhardwaj, A., Joss, L., Casjens, S., and Cingolani, G. (2007) Role of gene 10 protein in the hierarchical assembly of the bacteriophage P22 portal vertex structure. *Biochemistry* **46,** 8776–8784
20. Bhardwaj, A., Olia, A. S., Walker-Kopp, N., and Cingolani, G. (2007) Domain organization and polarity of tail needle GP26 in the portal vertex structure of bacteriophage P22. *J. Mol. Biol.* **371,** 374–387
21. Koksal, A. C., Nardozzi, J. D., and Cingolani, G. (2009) Dimeric quaternary structure of the prototypical dual specificity phosphatase VH1. *J. Biol. Chem.* **284,** 10129–10137
22. Nardozzi, J., Wenta, N., Yasuhara, N., Vinkemeier, U., and Cingolani, G. (2010) Molecular basis for the recognition of phosphorylated STAT1 by importin α5. *J. Mol. Biol.* **402,** 83–100
23. Schuck, P. (2000) Size-distribution analysis of macromolecules by sedimentation velocity ultracentrifugation and lamm equation modeling. *Biophys. J.* **78,** 1606–1619
24. Semenyuk, A. V., and Svergun, D. I. (1991) GNOM–a program package for small-angle scattering data processing. *J. Appl. Crystallogr.* **24,** 537–540
25. Svergun, D. I. (1999) Restoring low resolution structure of biological macromolecules from solution scattering using simulated annealing. *Biophys. J.* **76,** 2879–2886
26. Wriggers, W. (2010) Using Situs for the integration of multi-resolution structures. *Biophys. Rev.* **2,** 21–27
27. Birmanns, S., Rusu, M., and Wriggers, W. (2011) Using Sculptor and Situs for simultaneous assembly of atomic components into low-resolution shapes. *J. Struct. Biol.* **173,** 428–435
28. Pettersen, E. F., Goddard, T. D., Huang, C. C., Couch, G. S., Greenblatt, D. M., Meng, E. C., and Ferrin, T. E. (2004) UCSF Chimera–a visualization system for exploratory research and analysis. *J. Comput. Chem.* **25,** 1605–1612
29. Afonine, P. V., Headd, J. J., Terwilliger, T. C., and Adams, P. D. (2013) New tool: phenix.real_space_refine. *Comput. Crystallogr. Newslett.* **4,** 43–44
30. Svergun, D. I., Barberato, C., and Koch, M. H. J. (1995) CRYSOL–a program to evaluate x-ray solution scattering of biological macromolecules from atomic coordinates. *J. Appl. Crystallogr.* **28,** 768–773
31. Otwinowski, Z., and Minor, W. (1997) Processing of x-ray diffraction data collected in Oscillation mode. *Methods Enzymol.* **276,** 307–326
32. Terwilliger, T. C., Dimaio, F., Read, R. J., Baker, D., Bunkóczi, G., Adams, P. D., Grosse-Kunstleve, R. W., Afonine, P. V., and Echols, N. (2012) phenix.mr_rosetta: molecular replacement and model rebuilding with Phenix and Rosetta. *J. Struct. Funct. Genomics* **13,** 81–90
33. Adams, P. D., Afonine, P. V., Bunkóczi, G., Chen, V. B., Davis, I. W., Echols, N., Headd, J. J., Hung, L. W., Kapral, G. J., Grosse-Kunstleve, R. W., McCoy, A. J., Moriarty, N. W., Oeffner, R., Read, R. J., Richardson, D. C., Richardson, J. S., Terwilliger, T. C., and Zwart, P. H. (2010) PHENIX: a comprehensive Python-based system for macromolecular structure solution. *Acta Crystallogr. D Biol. Crystallogr.* **66,** 213–221
34. Emsley, P., and Cowtan, K. (2004) Coot: model-building tools for molecular graphics. *Acta Crystallogr. D Biol. Crystallogr.* **60,** 2126–2132
35. Minassian, B. A., Andrade, D. M., Ianzano, L., Young, E. J., Chan, E., Ackerley, C. A., and Scherer, S. W. (2001) Laforin is a cell membrane and endoplasmic reticulum-associated protein tyrosine phosphatase. *Ann. Neurol.* **49,** 271–275
36. Christiansen, C., Abou Hachem, M., Janecek, S., Viksø-Nielsen, A., Blennow, A., and Svensson, B. (2009) The carbohydrate-binding module family 20–diversity, structure, and function. *FEBS J.* **276,** 5006–5029
37. Meekins, D. A., Raththagala, M., Husodo, S., White, C. J., Guo, H. F., Kötting, O., Vander Kooi, C. W., and Gentry, M. S. (2014) Phosphoglucan-bound structure of starch phosphatase Starch Excess4 reveals the mechanism for C6 specificity. *Proc. Natl. Acad. Sci. U.S.A.* **111,** 7272–7277
38. Lee, J. O., Yang, H., Georgescu, M. M., Di Cristofano, A., Maehama, T., Shi, Y., Dixon, J. E., Pandolfi, P., and Pavletich, N. P. (1999) Crystal structure of the PTEN tumor suppressor: implications for its phosphoinositide phosphatase activity and membrane association. *Cell* **99,** 323–334
39. Jackson, M. D., and Denu, J. M. (2001) Molecular reactions of protein phosphatases–insights from structure and chemistry. *Chem. Rev.* **101,** 2313–2340
40. Roy, A., Kucukural, A., and Zhang, Y. (2010) I-TASSER: a unified platform for automated protein structure and function prediction. *Nat. Protoc.* **5,** 725–738
41. Sorimachi, K., Le Gal-Coëffet, M. F., Williamson, G., Archer, D. B., and Williamson, M. P. (1997) Solution structure of the granular starch binding domain of *Aspergillus niger* glucoamylase bound to β-cyclodextrin. *Structure* **5,** 647–661
42. Sánchez-Martín, P., Raththagala, M., Bridges, T. M., Husodo, S., Gentry, M. S., Sanz, P., and Romá-Mateo, C. (2013) Dimerization of the glucan phosphatase laforin requires the participation of cysteine 329. *PLoS One* **8,** e69523
43. Xiao, J., Engel, J. L., Zhang, J., Chen, M. J., Manning, G., and Dixon, J. E. (2011) Structural and functional analysis of PTPMT1, a phosphatase required for cardiolipin synthesis. *Proc. Natl. Acad. Sci. U.S.A.* **108,** 11860–11865
44. Dukhande, V. V., Rogers, D. M., Romá-Mateo, C., Donderis, J., Marina, A., Taylor, A. O., Sanz, P., and Gentry, M. S. (2011) Laforin, a dual specificity phosphatase involved in Lafora disease, is present mainly as monomeric form with full phosphatase activity. *PLoS One* **6,** e24040
45. Liu, Y., Wang, Y., Wu, C., Liu, Y., and Zheng, P. (2006) Dimerization of Laforin is required for its optimal phosphatase activity, regulation of GSK3β phosphorylation, and Wnt signaling. *J. Biol. Chem.* **281,** 34768–34774
46. Dubey, D., and Ganesh, S. (2008) Modulation of functional properties of laforin phosphatase by alternative splicing reveals a novel mechanism for the EPM2A gene in Lafora progressive myoclonus epilepsy. *Hum. Mol. Genet.* **17,** 3010–3020
47. Wang, J., Stuckey, J. A., Wishart, M. J., and Dixon, J. E. (2002) A unique carbohydrate binding domain targets the lafora disease phosphatase to glycogen. *J. Biol. Chem.* **277,** 2377–2380
48. DePaoli-Roach, A. A., Contreras, C. J., Segvich, D. M., Heiss, C., Ishihara, M., Azadi, P., and Roach, P. J. (2014) Glycogen phosphomonoester distribution in mouse models of the progressive myoclonic epilepsy, Lafora disease. *J. Biol. Chem.* **290,** 841–850
49. Gayarre, J., Duran-Trío, L., Criado Garcia, O., Aguado, C., Juana-López, L., Crespo, I., Knecht, E., Bovolenta, P., and Rodríguez de Córdoba, S. (2014) The phosphatase activity of laforin is dispensable to rescue Epm2a$^{-/-}$ mice from Lafora disease. *Brain* **137,** 806–818